



HAL
open science

Temperature and velocity measurements in a buoyant flow induced by a heat source array on a vertical plate

Antoine Baudoin, Didier Saury

► **To cite this version:**

Antoine Baudoin, Didier Saury. Temperature and velocity measurements in a buoyant flow induced by a heat source array on a vertical plate. *Experimental Thermal and Fluid Science*, 2017, 88, pp.234-245. 10.1016/j.expthermflusci.2017.06.002 . hal-02134977

HAL Id: hal-02134977

<https://hal.science/hal-02134977>

Submitted on 19 Apr 2020

HAL is a multi-disciplinary open access archive for the deposit and dissemination of scientific research documents, whether they are published or not. The documents may come from teaching and research institutions in France or abroad, or from public or private research centers.

L'archive ouverte pluridisciplinaire **HAL**, est destinée au dépôt et à la diffusion de documents scientifiques de niveau recherche, publiés ou non, émanant des établissements d'enseignement et de recherche français ou étrangers, des laboratoires publics ou privés.

Temperature and velocity measurements in a buoyant flow induced by a heat source array on a vertical plate

Antoine Baudoin^a, Didier Saury^b

^a*Division for Electricity, Uppsala University, Box 534, 751 21, Uppsala, SWEDEN*

^b*Institut PPRIME-CNRS, ENSMA, Université de Poitiers, BP 40109, F-86961 Futuroscope Chasseneuil CEDEX, FRANCE*

Abstract

Heat source arrays are common in engineering applications. Natural convection is a reliable and silent cooling strategy. Therefore, an array of flush-mounted heat sources has been studied under conjugate conduction and natural convection condition. This studies was performed for a system with relatively large dimensions, typical for power electronics, and a modified Rayleigh number up to $2 \cdot 10^{10}$. A modular set of heaters was designed to vary the distribution of heat sources on the plate and investigate the influence of the spacing. Velocity and temperature were measured in the convective flow with particle image velocimetry and micro-thermocouple. The velocity field was analyzed with proper orthogonal decomposition. The first instabilities of the convective flows were described. The results gave a better understanding of the heat transfers in these configurations and are valuable for model validation.

Keywords: heat source array; conjugate natural convection; velocity measurements; particle image velocimetry; micro-thermocouple; proper orthogonal decomposition.

Nomenclature

ρ	Density	kg/m ³
λ_f	Fluid thermal conductivity	W/m.K
λ_s	Solid thermal conductivity	W/m.K
α	Thermal diffusivity	m ² /s
δT	Thermal boundary layer thickness	m
δV	Velocity boundary layer thickness	m
ν	Kinematic viscosity	m ² /s
θ	Dimensionless temperature	-
L	Heat source width	m

*Corresponding author

Email address: antoine.baudoin@m4x.org (Antoine Baudoin)

T	Temperature	K
T_{∞}	Ambient temperature	K
q''	Heat flux density	W/m ²
H	Heat source height	m
Nu	Nusselt number	-
Ra	Rayleigh number	-
Y^*	Dimensionless distance to the wall ($= y/H$)	-
Z^*	Dimensionless vertical coordinate ($= z/H$)	-
\tilde{Z}^*	Dimensionless conductive/convective length	-
ΔX	Horizontal spacing	m
ΔZ	Vertical spacing	m
BL	Boundary Layer	
PCB	Printed Copper Board	
PIV	Particle Image Velocimetry	
POD	Proper Orthogonal Decomposition	
RMS	Root Mean Square	

1. Introduction

5 The phenomenon of natural convection is present as soon as a temperature gradient appears in a fluid. It is therefore of importance in many engineering applications [1]. Arrays of heat sources are common configurations in systems such as electronics. Electrical losses in components give rise to cooling issues, for instance with power electronics for renewable energies [2].

10 Interests for conjugate natural convection grew with the development electronic. Miniaturization in microelectronics and the consequent increase in heat flux density made it necessary to optimize cooling. In 1995, an array of identical discrete heat sources was studied numerically and experimentally with conjugate conduction and natural convection [3]. The importance of 3D-effects was highlighted and a numerical model was validated for laminar steady conditions. 15 Based on these results, a parametric study was presented for the fluid/substrate thermal conductivity ratio and for the modified Rayleigh number ($< 10^9$) [4].

The thermal coupling between the sources in a array under natural convection is nonlinear and complex. A first optimization study was performed 20 for discrete heating with heaters of an infinite length and to solve the problem with a two-dimensional equations [5]. The convective flow driven by linear heat sources was studied experimentally in [6]. Similar problems with forced convection or with protruding sources have also been studied, like for instance in [7, 8].

25 An array of flush mounted sources with diverse sizes was studied experimentally and numerically in [9]. The purpose was to test different configurations in order to optimize the heat transfer. The influence of the spacing between identical heat sources on the overall thermal resistance has been studied for optimization purposes in [10].

30 A 3x3 heater array in an enclosure with liquid cooling has been studied numerically for low Rayleigh numbers ($< 10^8$) in [11]. It showed that, the local

Nusselt number presented important variations in space and the influence of the enclosure aspect ratio was studied. In [12], the orientation of the cavity was studied on the convective flow due to an array of heat source.

35 In [13] a problem with multiple non-identical sources was optimized at low Rayleigh number. The temperature was measured at the source and a non-dimensional distance parameter was introduced to implement a first order optimization strategy.

40 Artificial neural network was used together with genetic algorithm in [14] for an array of heaters with different sizes. The temperature excess was also experimentally studied at the source. The distribution of protruding heat sources in a vertical duct was optimized under forced convection with an ANN-GA approach in [15].

45 This type of problems has been the subject of several reviews [16, 17]. Most of the published work was conducted in the context of a sealed cavity. Steady flow and temperature has been a commonly used assumption. Despite all the available literature, a lack of flow measurements is mentioned in [6]. Experimental setups have been limited to temperature measurements. Besides, most of the work has been performed for low Rayleigh number and laminar regime.

50 This present study provides experimental results of the combined temperature, heat transfer and velocity measurements for a system with discrete heat sources with large dimensions (e.g. typical for power electronics components) and open boundaries. The dimensions result essentially in higher Rayleigh number which determine the flow regime. Considering the unstable character of natural convection [18], the fluctuations of the flows were also studied.

2. Method

2.1. Experimental setup

60 Figure 1 presents the experimental setup. All the tests were performed in a big glass chamber located inside an air conditioned room with a constant temperature. Nine rectangular heat sources were flush-mounted on one side of a vertical metal plate. The heat sources consisted of 3 rows and 3 columns of sources. An array of modular heat sources was designed in order to study the effect of the spacing between the heat sources (see Figure 2). The other side of metal plate is directly in contact with air and is cooled essentially by natural convection. The plate was chosen to have a low emissivity (approximately 0.1) in order to limit radiative effects.

65 The heat sources consisted of printed copper board (PCB) with an electrical resistance of around 0.5Ω . As shown in Figure 2 (right), a thermal sheet was placed between the PCB and the plate. It was used to insulate electrically while enhancing the thermal contact. Its thermal conductivity was 7 W/mK . A piece of polyurethane foam was mounted in the back of the PCB with a conductivity of 0.028 W/mK . A PVC plate was added on the back of the polyurethane foam in order to apply a uniform mechanical pressure. Pressure was applied with two screws with approximately 0.4 Nm on each.

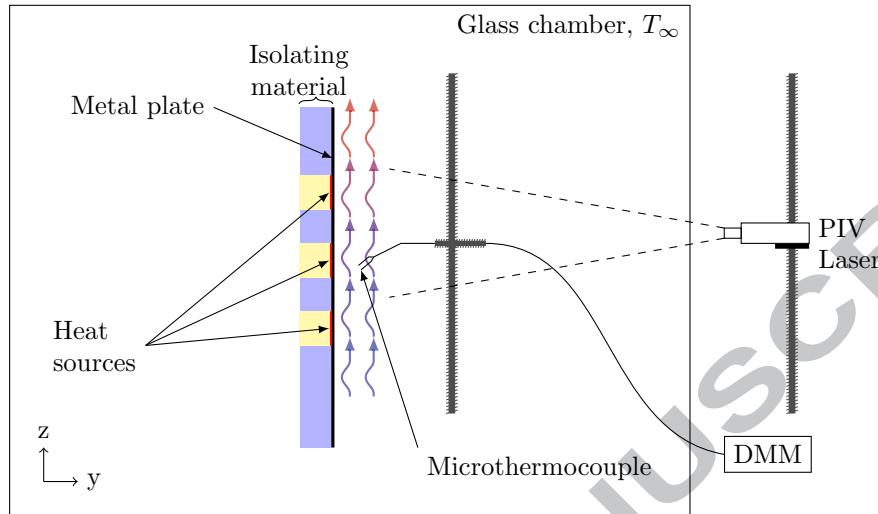


Figure 1: Schematic view of a middle plane of the setup.

Parameter	Value
Metal plate	200 x 150 cm
PCB heating plates (thickness)	5 x 10 cm (1,6 mm)
Thermal sheet thickness	0,2 mm
Polyurethane foam (thickness)	6 x 11 cm (40 mm)
PVC plate (thickness)	6 x 11 cm (5 mm)

Table 1: Dimensions of experimental setup

75 The rest of the backside of the plate was covered by a set of modular pieces
of thermally insulating materials. Extruded polystyrene foam, with a thermal
conductivity of 0.031 W/mK, was used to obtain adiabatic conditions while still
being able to change easily the position of the heat sources mounted on extruded
aluminum bars along which they could be moved. This insulating material was
80 chosen for its good mechanical properties.

All the heat sources were controlled by one single DC-supply unit. The
power dissipated by each heat source was balanced by tuning the resistances and
cables prior to the tests. A thermocouple of type T was installed at the centre
of the heaters, to monitor the temperature for each heat source connected to an
85 Agilent 34970 data acquisition unit with two 34901A cards, giving an accuracy
of $\pm 1\text{K}$.

2.2. Experimental protocol

At the beginning of the test, the sources were mounted against the metal
plate with a nano-screwdriver for a uniform thermal contact (approximately

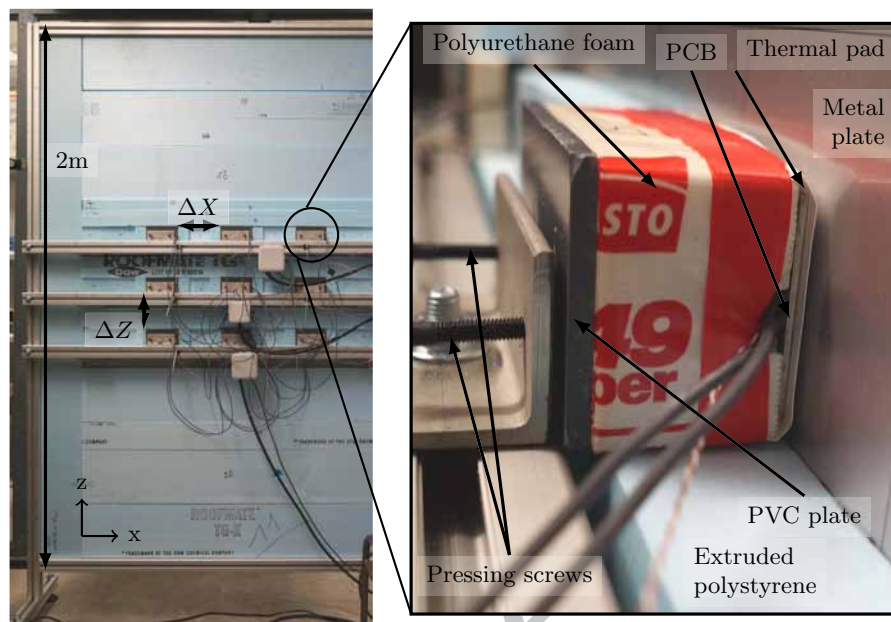


Figure 2: Experimental setup for study of a heat source array. The backside of the plate with heat sources and modular isolating pieces structure to change the spacing (left). One of the heat sources mounted on the back of the metal plate (right).

90 0.4 Nm). Because of the thermal expansion, the screws were retightened when the temperature had reached a permanent regime ($< 1\text{K}/30\text{min.}$). The velocity was first measured with Particle Imaging Velocimetry (PIV). Then, a microthermocouple used to measure the temperature. All measurements were performed for different distributions of the sources (i.e. horizontal and vertical spacings),
 95 as well as for different power levels. The two power levels corresponded to heat flux density of 1,1 and 2 kW/m^2 . PIV and micro-thermocouple measurements were conducted in the middle vertical plane.

2.2.1. Velocity measurements

The convective flow was measured with a double-pulsed laser (Nd-YAG) together with a dedicated Dantec SpeedSense 9040 CCD camera (see Figure 3).
 100 The camera and the laser are synchronized with a BNC 575 pulse generator. Both were placed outside the glass cavity not to perturb the convective flow. Shell Ondina Oil was used in a Laskin generator to seed the flow with 1-5 μm oil particles. The velocity vectors were calculated using the commercial software
 105 DynamicStudio, with a filter on correlation peak height ratio. An adaptive interrogation window of 64×64 to 16×16 pixels was used with an overlapping of 50%. The distance between two contiguous vectors was therefore 0.92 mm.

Pictures were acquired during 100 s (determined with a convergence test)

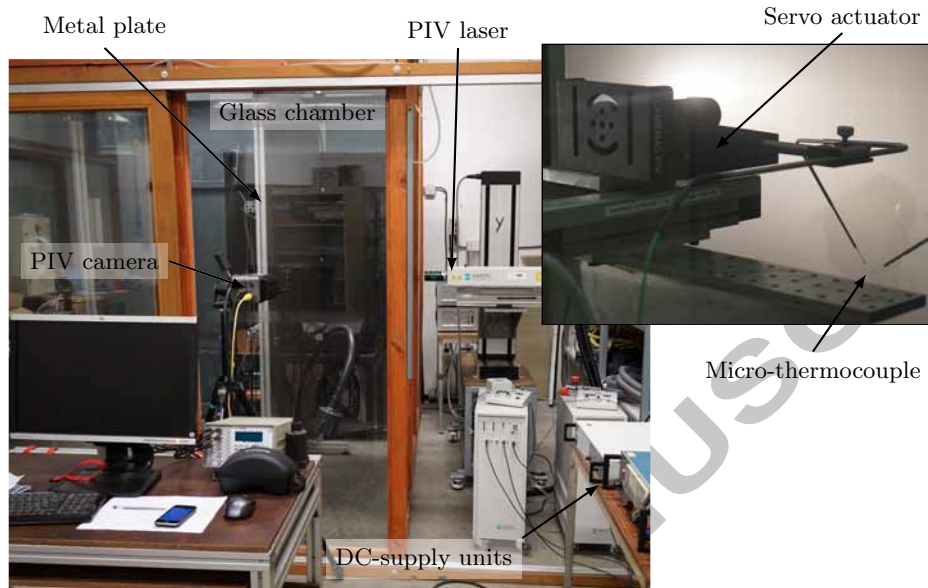


Figure 3: PIV and micro-thermocouple measurements. All equipment was placed outside the glass chamber not to disturb the convective flow.

at a frequency of 50 Hz. The delay between the two lasers pulses was set 2 ms
 110 to match the velocity in the boundary layer. To obtain good results in both
 the low-velocity region (far from the wall) and the high velocity region (in the
 boundary layer), the vector calculation was performed twice. First, the pairs
 of frames were used (i.e. with a time step of 2 ms) and then the first frame
 of consecutive pairs (i.e. with a time step of 20 ms). The two fields were later
 115 combined by selecting the best vectors at each point with a criteria based on
 the norm of the velocity.

The first analysis of the results showed a very low mean velocity in the
 near wall regions. Indeed a detailed inspection of the pictures revealed that the
 particle density was low in these regions. No particle was present on a majority

Parameter	Value
Pictures size	1632 x 800 pixel
Pictures size	186 x 94 mm
Scaling factor	0.115 mm/pixel
Delay between laser pulses	2 ms
Acquisition frequency	50 Hz
Focal length of the objective	100 mm

Table 2: Settings for PIV

120 of the pictures. Therefore a special treatment was used for these regions, to eliminate the zero-velocity vectors.

To cover the entire heated region, both the camera and the lasers were mounted on a linear servo actuator for movement in the vertical direction (see Figure 1). The measurement were carried out repeatedly at different vertical
125 positions. Finally, edge detection was applied to the pictures using a Gaussian gradient threshold method. It was done to straight up the wall in the image in order to merge the results properly.

2.2.2. Temperature measurements

A thermocouple of diameter 12,7 micrometer was used to measured tempera-
130 ture in the air flow. This K-type thermocouple was mounted on a multi-axes linear servo actuators system for movement in the vertical- and y-direction. In the direction normal to the plate, the precision of the moving axis was $\pm 0.02\text{mm}$. The thermocouple was first moved manually to touch the plate by using a scope for precision. The position was then controlled by a computer with the soft-
135 ware Labview which also logged the temperature measurement. In this way the measurements for an horizontal temperature profile were automated. The data acquisition was delayed with several seconds after each displacement to avoid vibrations.

The frequency acquisition was 50 Hz during 100 s at each point. The density
140 of measurement points was set in the direction normal to the wall as a decreasing function of the distance to wall. Five points were taken within the first millimeter, as it was shown to be sufficient to obtain a high correlation factor for the linear regression ($r^2 > 0.99$) to determine the wall heat flux. Far from the wall the points were spaced by 1 cm.

The ambient temperature, T_∞ , was measured with a PT100 sensor immersed
145 in water. The data were acquired with a multimeter NI PXI 1031 installed in a NI 4071 DMM unit. It gave a sensitivity of ± 0.01 K for the chosen logging frequency. The standard deviation for the temperature measurement is below 0.3 K for each dataset (i.e. a time serie for one given position of the thermocou-
150 ple). This is due to fluctuations of temperature. The temperature measurement was zeroed before heating and only temperature difference was measured (i.e. relative to the PT100 ambient measurement). A in-situ calibration ensures an uncertainty below 0,5 K for the measured time-averaged temperature difference.

2.3. Data analysis

155 The dimensionless temperature is defined in Equation 1. It is used to define the dimensionless local heat transfer coefficient, the Nusselt number Nu , as shown in Equation 2.

$$\theta = \frac{T - T_\infty}{q'' \cdot H / \lambda_f} \quad (1)$$

$$Nu = \frac{\partial \theta}{\partial Y^*} \quad (2)$$

A Monte-carlo simulation was run with a normal law on the linear regression that gives the Nusselt number. As a results, the error could be estimated for each horizontal profile given uncertainties for temperature and position (see
 160 previous section). The modified Rayleigh number is proposed in Equation 3. It is based on Equation 1 and the characteristic length ΔZ .

$$Ra_{\Delta z} = \frac{g \cdot \beta \cdot (q'' \cdot H / \lambda_f) \cdot \Delta Z^3}{\alpha \cdot \nu} \quad (3)$$

In order to analyze the velocity fields, a Proper Orthogonal Decomposition (POD) was performed. This method was applied on each height section separately, as the acquired data correspond to different time series. Given the
 165 dimension of the field ($> 10\,000$ vectors) and the number of time steps ($< 5\,000$), the snapshots method was selected [19]. To calculate the mean field and subtract it, only valid vectors were taken into account (see filters described in Section 2.2.1).

The snapshots matrix is defined as $U = (u_t^i)$ where u_t^i is the velocity fluctuation at the i -th point and for the t -th timestep. The eigenvectors of the auto-correlation matrix $C = U \cdot U^t$ are used to define the fluctuation modes as linear combinations of the snapshots. The eigenvalues represent the kinetic energy of the modes. The velocity field can then be reconstructed by using only
 170 the most energetic modes.

3. Results

The modified Rayleigh number ranged from $2,9 \cdot 10^8$ to $1,9 \cdot 10^{10}$, depending on the distribution layout and the input power (≈ 6.5 W to ≈ 12 W). In this section, the experimental results are first presented to give a complete description
 180 of the convective flow. These results are then analyzed to quantify the local heat transfer, the boundary layers thickness and the instability of the flow. All results are presented for the vertical mid-plane (i.e. symmetry plane) of the setup.

3.1. Temperature and velocity measurements

The convective phenomenon was fully characterized by the temperature and the velocity measurements inside the flow. The results are presented in this section to describe the conjugate convective flow. The vertical profiles presented
 185 in the following were measured along a vertical line at the centre of the middle column of heat sources.

3.1.1. Wall temperature

The dimensionless temperature is shown in Figure 4. The temperature elevation was measured to be up to nearly 100 K. This high value was logically obtained for a distribution dense in both vertical and horizontal directions. The lowest temperatures were measured for large horizontal and vertical spacing.
 190 The maximum temperature was almost the same for a wide horizontal spacing

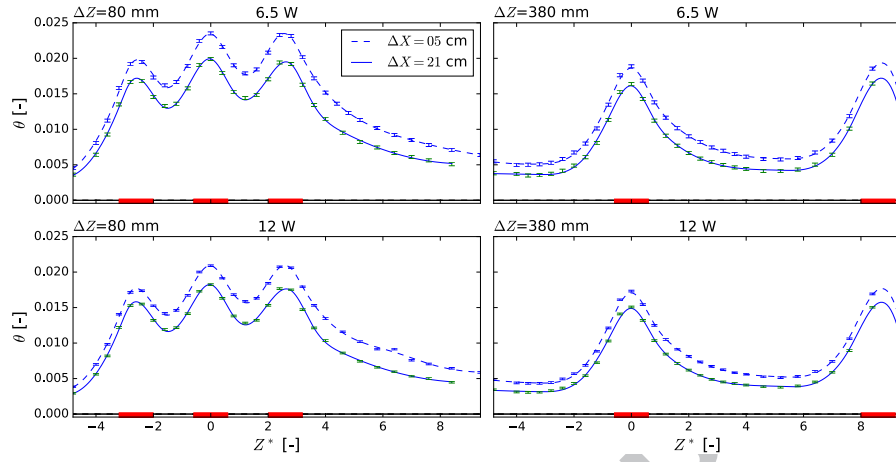


Figure 4: Dimensionless wall temperature for different distributions and different powers. The plain lines correspond to a larger horizontal spacing. The reference position was chosen at the centre of the central heat source.

/ low vertical spacing as for the opposite. This indicates the possibility to define an optimal configuration giving the best cooling on the smallest area.

The wall temperature at the lower heat sources was lower than for the upper row, indicating the effect of convective heat transfers. The middle row exhibited high temperature due to conductive thermal interaction between the sources.

When moving away from the centre of the heaters, the temperature decreased rapidly. The rate of this decrease can be compared with the dimensionless length defined in Equation 4. For a spacing smaller than \tilde{Z}^* , the temperature between the sources do not drop as in Figure 4. This drop appears and increases when the vertical spacing is increased. It can be already observed for a vertical spacing of 80 mm (slightly above \tilde{Z}^*) and is significant for a spacing of 380 mm.

$$\tilde{Z}^* = \frac{\lambda_s \cdot e}{\lambda_f \cdot H} \approx 1 \quad (4)$$

The ratio \tilde{Z}^* represents the importance of the conductive heat transfer in the substrate and against the convective heat transfer at the wall. An infinite value corresponds to an isothermal plate. In this case, the area covered by the heat sources is at a uniform temperature and the position of heat sources could not be distinguished in the results. On the contrary, a low value would result to a uniform heating configuration over the regions of each separate heat source. The considered case is thus perfectly intermediate. The length \tilde{Z}^* proposed here is believed to characterize the conjugated heat transfer better than the thermal conductivity ratio used in [4, 20].

The above mentioned decrease of the temperature was quicker downstream of the sources than upstream because of the convective flow which transports

heat upwards. The dissipated power did almost not affect the wall temperature profiles.

220 When the horizontal spacing was wider, an overall increase of the temperature was observed, but the shape of the profiles is almost not modified. However, the horizontal spacing had a little more impact downstream far from the sources where the temperature decrease was slowed down. When reducing the horizontal spacing, the configuration became 2-dimensional and resembled heating bands.
225 This inhibits horizontal heat transfer.

3.1.2. Vertical mid-plane Velocity field

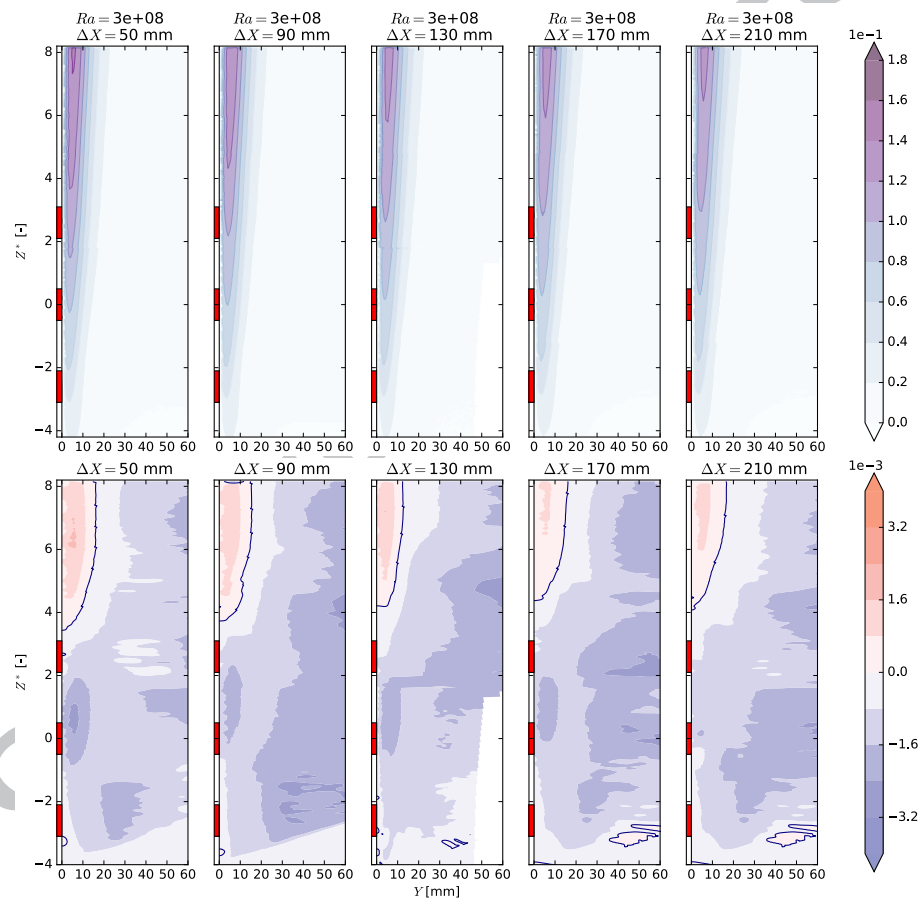


Figure 5: Dimensionless vertical (top) and horizontal (bottom) velocity components at varying horizontal spacing for a fixed vertical spacing ($\Delta Y = 80$ mm). The blue lines show the limit between positive and negative horizontal velocity.

The complete velocity field was successfully obtained from the separate PIV

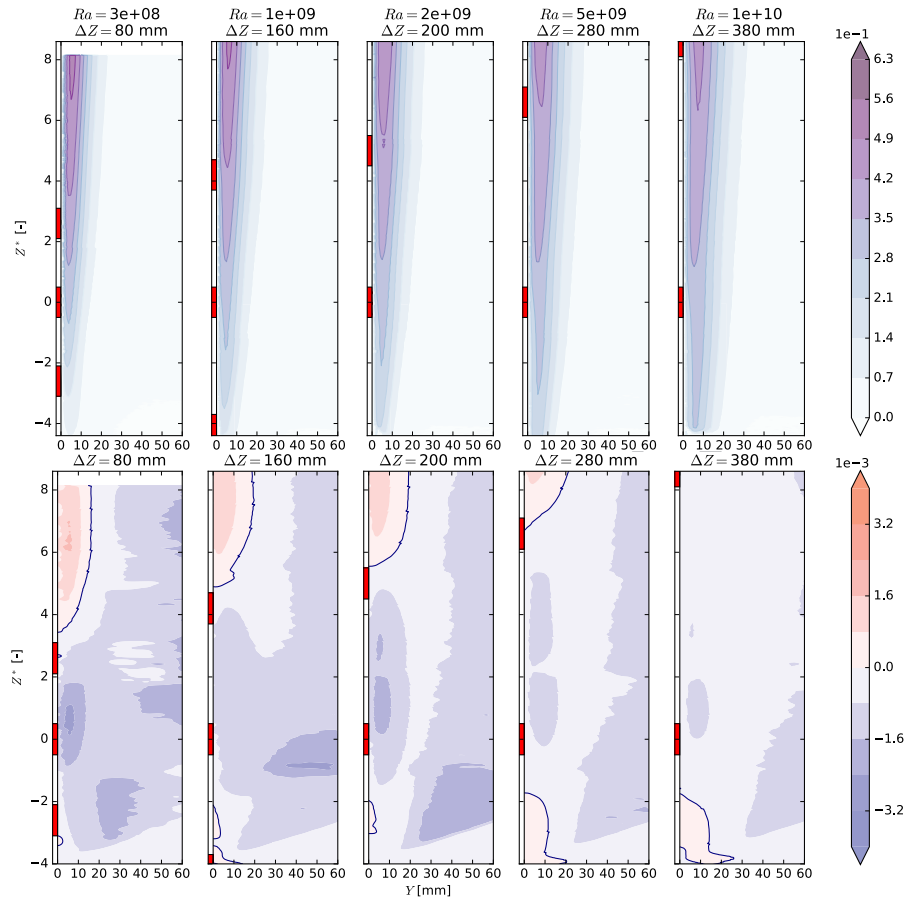


Figure 6: Absolute vertical (top) and dimensionless horizontal (bottom) velocity components at varying vertical spacing for a fixed horizontal spacing ($\Delta X = 50$ mm). The blue line shows the limit between positive and negative horizontal velocity.

fields. Figures 5 to 6 (top graphs) show that the flow is accelerating along the plate as it gets heated-up. The horizontal spacing had an indirect influence on the velocity (see Figure 5). It is due to an overall higher temperature. However, the horizontal spacing had a limited effect on the structure of the flow.

In Figure 6, it can be seen that the vertical spacing had a much greater effect on the velocity. It validates the definitions of the modified Rayleigh number (see Equation 3). The boundary layer becomes thicker and longer for a wider vertical spacing. The acceleration is slower for wide vertical spacing.

The description of the fields is also supported by the profiles shown in Figure 7. On these profiles, it can be seen that the temperature profiles are modified downstream of the heat sources. The slope becomes positive near the wall.

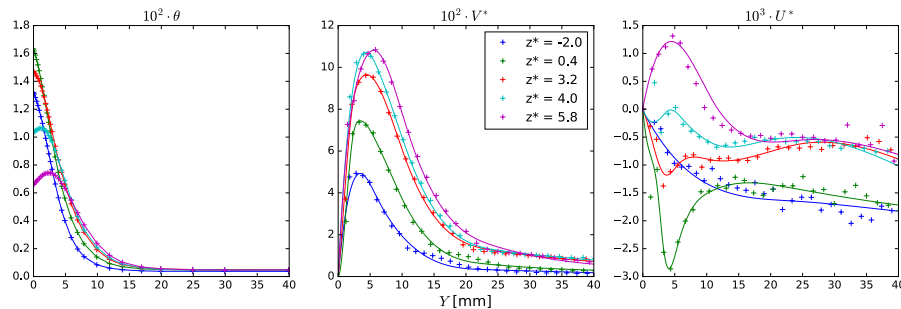


Figure 7: Temperature (left), vertical velocity (middle) and horizontal velocity (right) horizontal profiles. Results obtained for a low vertical spacing. The positions of the profiles correspond to the upper limit of the heat sources ($Z^* = -2, 0.4, 3.2$) and downstream of the last heat source ($Z^* = 4.0, 5.8$). $\Delta Y = 80$ mm and $\Delta X = 50$ mm.

Likewise, the horizontal velocity profiles are inverted for the profiles above the upper row. This correspond to the region of positive horizontal velocity component (see bottom graphs in Figures 5 and 6). The horizontal component of the velocity was much lower than the vertical one, except from the region far from the wall. This component was oriented towards the wall except from a region near the wall and downstream of the last heat source (see bottom graphs in Figures 5 and 6). Right after the upper source, the suction stopped and the fluid was ejected. The fluid is cooled by the plate and the buoyancy forces becomes weaker. The region of positive horizontal component is moving with the upper row when increasing the vertical spacing. When the fluid is accelerated (due to heating from the wall), we can observe a suction toward the wall. On the contrary, when then fluid is decelerated the flow is rejected. The flow becomes a wall jet and the energy is dispersed (we can see than the boundary layers is widening). Good agreement between the observations on temperature and velocity features. Cooling by the wall is noticeable in the upper profiles and explains the rejected flow. This will be analyzed further in the next section.

3.2. Analysis

3.2.1. Nusselt number and boundary layer thickness

First of all, a linear regression was performed on the temperature measurement points closest to the wall in order to determine the dimensionless temperature gradient. The Nusselt number (see Equation 2) is shown in Figure 8. For illustrative purposes, it can be translated into a convection heat transfer coefficient of up to 6.5 W/Km² (with H as a characteristic length). The Nusselt number was positive in the regions close to the heaters and decreased rapidly when moving away from them. For a tight layout in the vertical direction, the Nusselt number was positive in the whole region covered by heat sources.

In the case of a wider vertical spacing, the Nusselt number became negative between the sources, indicating an inversion of the thermal boundary layer. In

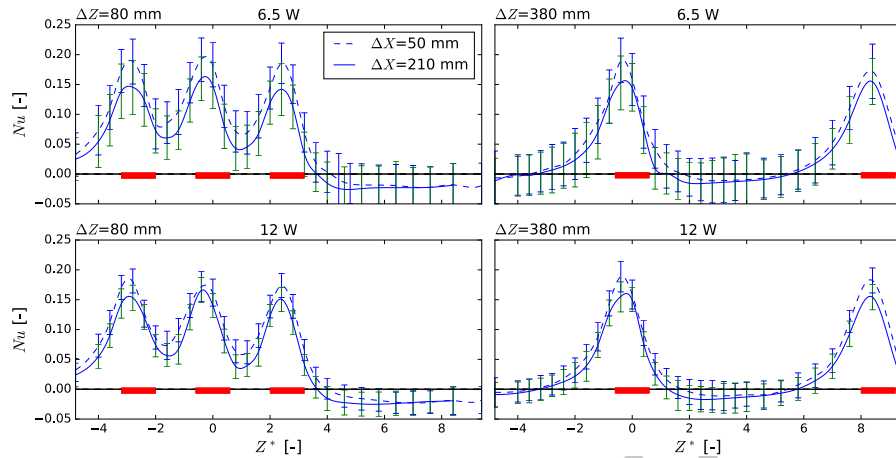


Figure 8: Nusselt number for different distributions and different powers. The plain lines correspond to a larger horizontal spacing.

these regions, the plate was heated by the fluid. This inversion occurred quickly downstream of the sources: less than $H/2$ in some cases. In fact, this feature was earlier and more pronounced for a layout tight in the horizontal direction. The horizontal spacing only slightly influenced the Nusselt number far from the source, but a noticeably higher Nusselt number was obtained at the heat source for a smaller spacing. The region with a positive Nusselt was limited to roughly $4H$ in some cases.

For a large vertical spacing, the Nusselt number was locally similar for the middle and the upper source. A comparison is shown in Figure 9 for the middle and the upper row. This indicates that, from a cooling perspective, this spacing is large enough to consider the source to be in similar conditions. In other words, no benefit can be expected from a further increase of the spacing.

The thickness of the thermal and velocity boundary layers (BL) was evaluated. These results are shown in Figures 10 and 11. The thickness was defined as the distance from the wall for which the temperature or the velocity had decreased by 50%. The layers were between 2 and 12 mm thick (thermal) and 8 to 20 mm (dynamic). The BL were thinnest close to the heat sources and thicker far from the heat sources.

The Figure10 shows how the kinetic BL is progressively modified from a constantly increasing thickness to a piecewise increasing and decreasing thickness when the vertical spacing is widened. For a layout tight in the vertical direction the velocity BL thickness increased almost constantly

In all cases, a larger horizontal spacing reduced the BL thickness. It also leads to a more rapidly increasing thickness downstream of the sources but no difference near the sources. The thermal BL thickness successively decreased in the heated region and increased between the heat sources for a larger spacing.

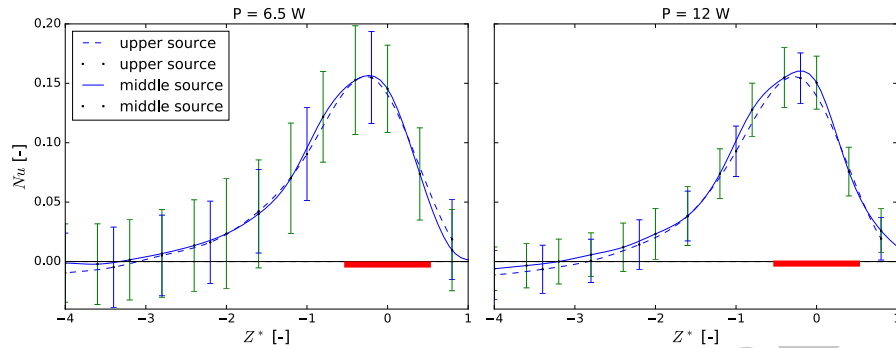


Figure 9: Nusselt number the middle and upper heat source. $\Delta Y = 380$ mm and $\Delta X = 210$ mm.

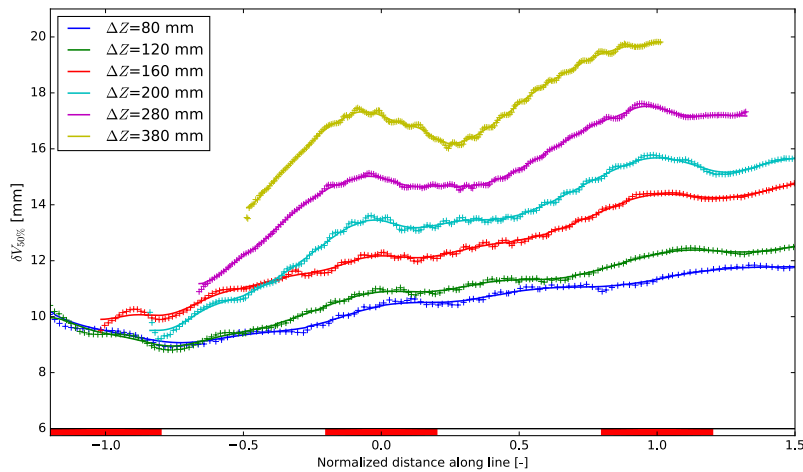


Figure 10: Velocity boundary layer thickness for an increasing vertical spacing ($\Delta X = 50$ mm). The horizontal axis is normalized by the vertical spacing for comparison.

The thermal BL presented wider variations than the kinetic one, especially for a large vertical spacing.

In the proximity of the heaters, both layers become thinner but the narrowing of both BLs is not in phase. The thermal BL thickness reaches its minimal value at the beginning of the heat source. On the contrary, the dynamic BL thickness is minimal downstream of the heated region.

An increase of dissipated power leads to slightly thinner boundary layers.

However, the shape of the curves was not changed.

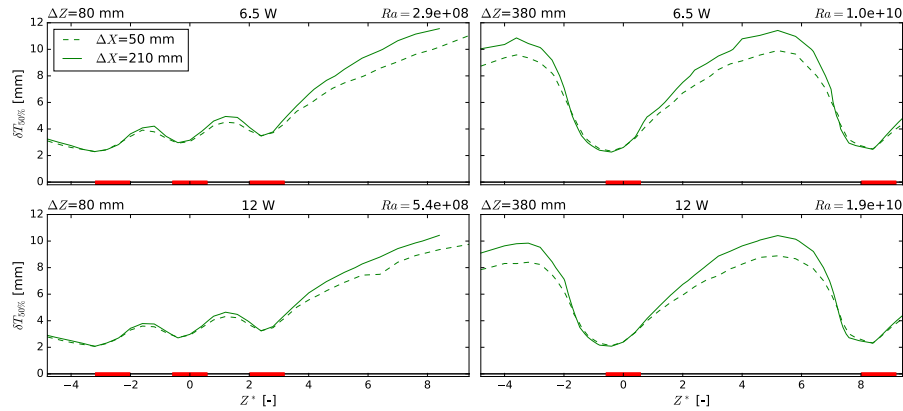


Figure 11: Thermal boundary layer thickness. The dashed and the plain lines show results obtained for a small and a large horizontal spacing, respectively.

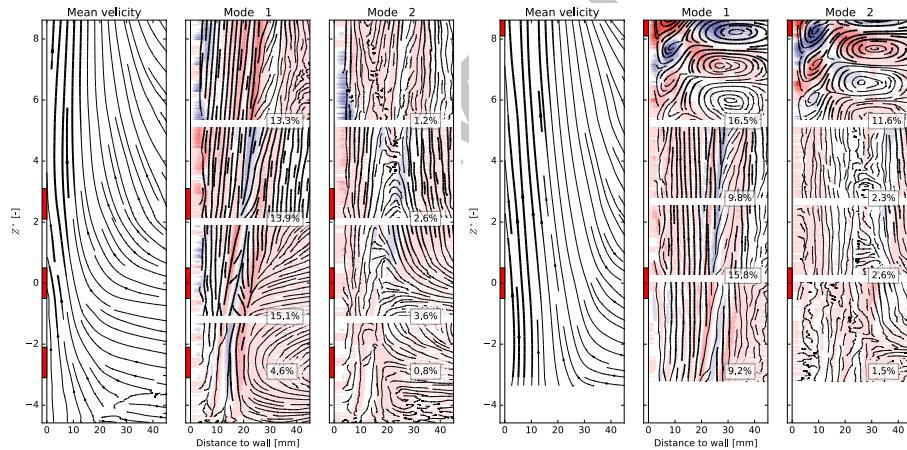


Figure 12: Streamlines for the mean velocity field and the 2 firsts modes from the POD analysis. The colorscale represents the rotational of the velocity. Tight layout in the vertical direction (left) and sparse layout (right).

3.2.2. Flow stability

As shown in Figure 12, the dominant POD-modes for most of the distributions and powers displayed straight lines at the limit of the velocity boundary layer. This corresponds to an acceleration/deceleration in the border of the layer. While no instabilities could be observed at modified Rayleigh number below 10^{10} (stationary laminar flow), rotational features were present in Figure 12 (right) for the highest Rayleigh number. These structures were moving upwards with the flow as illustrated in Figure 13. The structures are Tollmien-Schlichting

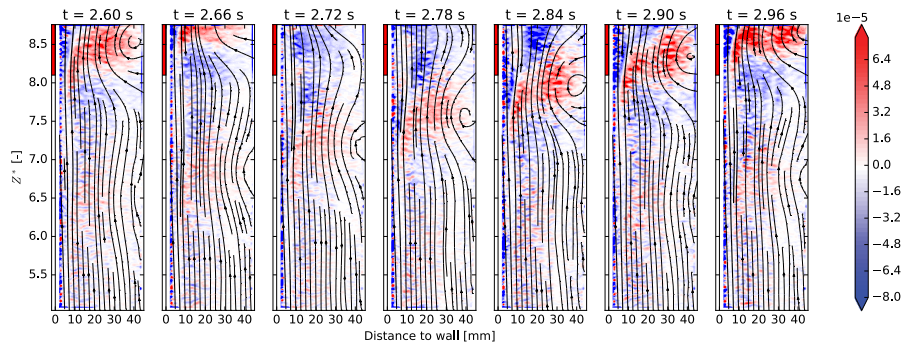


Figure 13: Example of time-series for the Q-criterion calculated for the reconstructed velocity field (50 modes used for 60% of the total energy)

propagating waves and appeared periodically as in the sequence of 0.3 s shown
 310 in Figure 13. The rotational features appeared at around $Z^* = 6$ downstream
 of the central source. Below that, no clear signal could be detected on the
 Q-criterion.

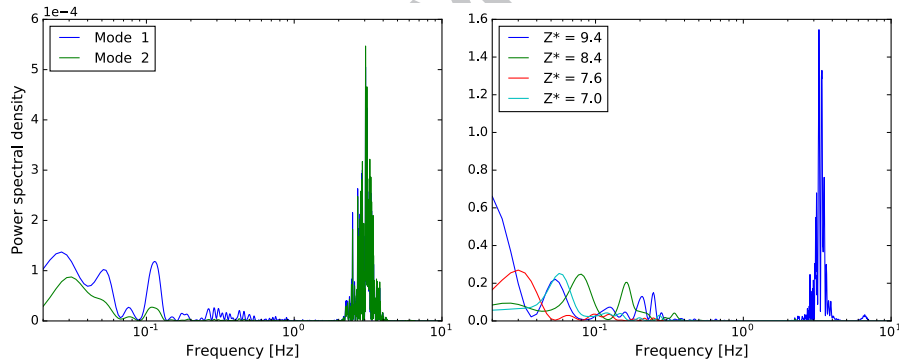


Figure 14: Fourier analysis for the POD modes (left) and for the corresponding temperature
 (right). The second one is shown for different positions in height ($y = 2.5$ mm). Results
 obtained for a tight layout at higher power at the top source. $Ra_{\Delta Z} = 2 \cdot 10^{10}$

The spectral analysis of the second type of modes (i.e. rotational in the upper
 region) is shown Figure 14. The results exhibit a clear peak for the velocity
 315 modes and a similar peak for the temperature. No results are shown for sparse
 distributions or for lower Rayleigh Number, because the spectra did not present
 any clear signals. The peak observed for the temperature is centered around
 3.3 Hz and is spread between 2.5 and 4 Hz, depending on the position. The first
 harmonic was also identified. A smaller and narrow peak is seen at 2.2 Hz closer
 320 to the wall. Both features were only present at the highest positions. In the

results from the POD analysis, the observed peak is at slightly lower frequency and is centered around 3.0 Hz. The results also suggest signals at low frequency (≈ 0.1 Hz and below) for both the temperature and the velocity.

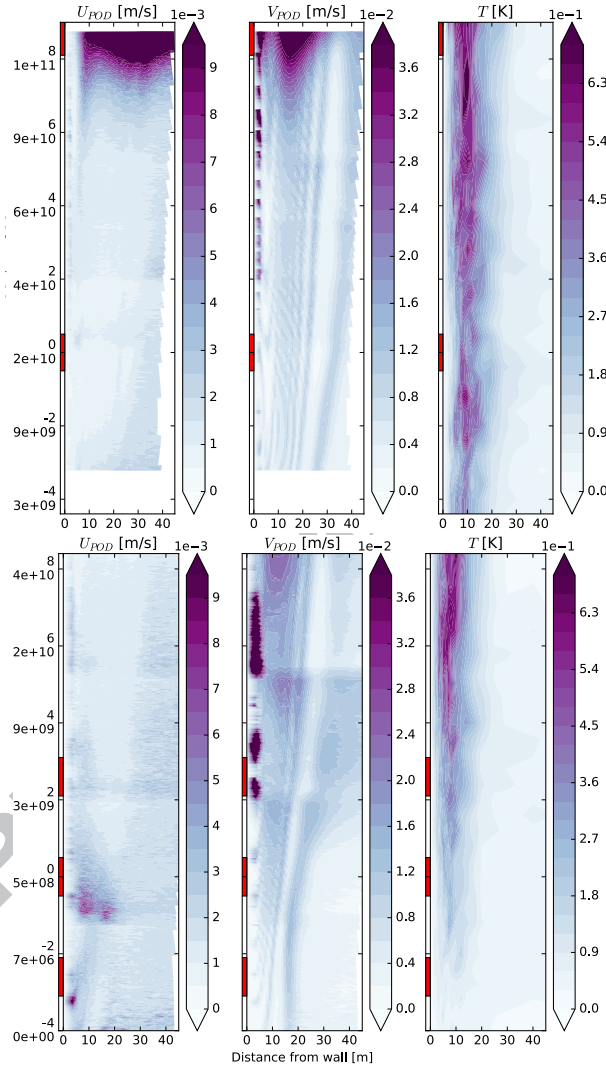


Figure 15: RMS-value for the velocity components before and after the POD treatment, as well as for the temperature (right). The upper figure shows the results for a low horizontal spacing and the lower one shows the results for the large horizontal spacing. The local Rayleigh number Ra_z is calculated with the position from the first heaters row. (100 modes used out of 4500)

The POD-filtered velocity fields were used to calculate the RMS value for each component. The results presented in Figure 15, show that the POD tech-

nique was successfully used to reduce the noise in the low-velocity regions. The RMS value is increasing in the boundary layer with the height and reached its maximum at the upper heat source. These results are in good agreement with the previous observations of rotational features appearing at $Z^* = 6$ in the firsts
 330 modes. A weaker feature also appeared in the region close to the heat sources, even for a low vertical spacing.

The RMS value for the temperature (right) displays larger spatial disparities. It increased continuously in the flow, even downstream of the sources. The RMS values for the temperature and the velocity appear to be only weakly correlated.
 335 These results are helpful for validating the turbulence in models as it is a major source of numerical uncertainties in case of natural convection. The RMS values are low for all configurations with a modified Rayleigh number below 10^{10} . Above this value, the RMS values increases rapidly in the upper part of the flow (local $Ra_z = 10^{11}$, see Figure 15). These observations support the introduction
 340 of the vertical spacing in the Rayleigh number.

A limited number of configurations could be tested in this study, as it was preferred to investigate the influence of a variety of parameters (the experimental procedure is time consuming). It is suggested that future work could focus on one single parameter (e.g. the vertical spacing which was showed to have a major
 345 effect of the convection flow) to perform a more detailed parametric sweep.

4. Conclusion

i/ The convective flow has been thoroughly described by temperature and velocity measurements in the flow. The influence of several parameters was investigated. The horizontal and vertical spacing between the heat sources as
 350 well as the dissipated power were varied. The vertical spacing was shown to have the greater impact on the convective flow and the heat transfer. These experimental data give an understanding of the thermal interaction between the heat sources. In particular, velocity measurements in this study are unique.

ii/ In a dense layout, the heat flux density is increased (i.e. better utilization
 355 of the area) but the temperature reaches values potentially harmful for the components. On the contrary, a sparse distribution of the heat sources gives lower temperature but at the price of a large covered area. So it appears that there is a necessity for a trade-off. Extreme cases have been studied here and give a frame for validation of models covering a range of distributions for optimization
 360 of a wide variety of cooling problems.

iii/ When the vertical spacing is significantly larger than the dimensionless conductive/convective length, the heat transfer was locally similar for the middle and the upper row for a sparse layout, although the velocity field was very
 different.

iv/ The horizontal spacing was shown to have only a limited influence on
 365 the temperature profiles and the flow. This observation tends to validate a posteriori the choice, made in many previous studies such as [5], to treat the optimization of the spacing as a two-dimensional problem. However, the effect of this parameter can not be completely neglected for high accuracy.

370 v/ The power level and the dimensions in this study reached values for
which the flow started transitioning. The critical modified Rayleigh number
was around $2 \cdot 10^{10}$. The temporal behavior of the flow was highlighted and
instabilities were discussed. All these results can be highly valuable to include
turbulent effects in numerical model.

375 Acknowledgments

This work was supported by SweGRIDS, KIC InnoEnergy and StandUP for
Energy. The authors also want to thank Bo Zhu, student at ENSMA.

- 380 [1] A. Baïri, E. Zarco-Pernia, J.-M. G. De María, A review on natural convec-
tion in enclosures for engineering applications. the particular case of the
parallelogrammic diode cavity, *Applied Thermal Engineering* 63 (1) (2014)
304–322.
- [2] A. Baudoin, C. Boström, Thermal modelling of a passively cooled inverter
for wave power, *Renewable Power Generation, IET* 9 (4) (2015) 389–395.
- 385 [3] T. Heindel, S. Ramadhyani, F. Incropera, Conjugate natural convection
from an array of discrete heat sources: part 1—two-and three-dimensional
model validation, *International Journal of Heat and Fluid Flow* 16 (6)
(1995) 501–510.
- [4] T. Heindel, F. Incropera, S. Ramadhyani, Conjugate natural convection
from an array of discrete heat sources: part 2—a numerical parametric
390 study, *International journal of heat and fluid flow* 16 (6) (1995) 511–518.
- [5] A. da Silva, S. Lorente, A. Bejan, Optimal distribution of discrete heat
sources on a wall with natural convection, *International Journal of Heat
and Mass Transfer* 47 (2) (2004) 203 – 214. doi:http://dx.doi.org/10.
1016/j.ijheatmasstransfer.2003.07.007.
- 395 [6] M. Habib, S. Said, T. Ayinde, Characteristics of natural convection heat
transfer in an array of discrete heat sources, *Experimental Heat Transfer*
27 (1) (2014) 91–111.
- [7] G. Sultan, Enhancing forced convection heat transfer from multiple pro-
truding heat sources simulating electronic components in a horizontal chan-
400 nel by passive cooling, *Microelectronics Journal* 31 (9–10) (2000) 773 – 779.
doi:http://dx.doi.org/10.1016/S0026-2692(00)00058-6.
- [8] M. Hajmohammadi, S. Nourazar, A. Campo, S. Poozesh, Optimal discrete
distribution of heat flux elements for in-tube laminar forced convection,
405 *International Journal of Heat and Fluid Flow* 40 (2013) 89 – 96. doi:
http://dx.doi.org/10.1016/j.ijheatfluidflow.2013.01.010.

- [9] S. Durgam, G. Ramanjaneyulu, S. Venkateshan, T. Sundararajan, A numerical and experimental study of optimal distribution of discrete heat source array cooled by natural and forced convection, Proceedings of First TFESC-12696, Begell House.
- 410 [10] A. Baudoin, D. Saury, B. Zhu, C. Boström, Experimental optimization of passive cooling of a heat source array flush-mounted on a vertical plate, *Energies* 9 (11) (2016) 912.
- [11] S. Tou, C. Tso, X. Zhang, 3-d numerical analysis of natural convective liquid cooling of a 3×3 heater array in rectangular enclosures, *International journal of heat and mass transfer* 42 (17) (1999) 3231–3244.
- 415 [12] C. Tso, L. Jin, S. Tou, X. Zhang, Flow pattern evolution in natural convection cooling from an array of discrete heat sources in a rectangular cavity at various orientations, *International Journal of Heat and Mass Transfer* 47 (19–20) (2004) 4061 – 4073. doi:<http://dx.doi.org/10.1016/j.ijheatmasstransfer.2004.05.022>.
- 420 [13] T. Sudhakar, C. Balaji, S. Venkateshan, A heuristic approach to optimal arrangement of multiple heat sources under conjugate natural convection, *International Journal of Heat and Mass Transfer* 53 (1–3) (2010) 431 – 444. doi:<http://dx.doi.org/10.1016/j.ijheatmasstransfer.2009.09.013>.
- 425 [14] T. K. Hotta, S. P. Venkateshan, Optimal distribution of discrete heat sources under natural convection using ann-ga based technique, *Heat Transfer Engineering* 36 (2) (2015) 200–211.
- [15] T. Sudhakar, A. Shori, C. Balaji, S. Venkateshan, Optimal heat distribution among discrete protruding heat sources in a vertical duct: a combined numerical and experimental study, *Journal of Heat Transfer* 132 (1) (2010) 011401.
- 430 [16] H. F. Öztop, P. Estellé, W.-M. Yan, K. Al-Salem, J. Orfi, O. Mahian, A brief review of natural convection in enclosures under localized heating with and without nanofluids, *International Communications in Heat and Mass Transfer* 60 (2015) 37–44.
- 435 [17] G. Narasimham, Natural convection from discrete heat sources in enclosures: an overview, *Vivechan Int J Res* 1 (2010) 63–78.
- [18] D. Saury, A. Benkhelifa, F. Penot, Experimental determination of first bifurcations to unsteady natural convection in a differentially-heated cavity tilted from 0° to 180° , *Experimental Thermal and Fluid Science* 38 (2012) 74–84.
- 440 [19] M. Bergmann, L. Cordier, J.-P. Brancher, Optimal rotary control of the cylinder wake using proper orthogonal decomposition reduced-order model, *Physics of Fluids* 17 (9). doi:<http://dx.doi.org/10.1063/1.2033624>.
- 445

- [20] R. Ali, K. El-Shazly, Optimal location of a heat source mounted in a substrate cooled by natural convection, *Al-Azhar University Engineering Journal*, JAUES 3 (11) (2008) 217–229.

ACCEPTED MANUSCRIPT

Highlight for “Temperature and velocity measurements in a buoyant flow induced by a heat source array on a vertical plate”:

- Temperature and velocity were measured for discrete heating and free convection.
- Vertical spacing in the array has the largest effect on the flow.
- Nu is similar over the rows for spacing larger than a convection/conduction length.
- The flow becomes unsteady for a critical modified Ra of $2 \cdot 10^{10}$.
- 3Hz travelling waves appears at the upper row in the border of the layers.